


## Preparation and Tribological Properties of a Superhydrophobic TB6 Titanium Alloy

Jialiang Guo<sup>a</sup> , Fang Wang<sup>a,b,c,d</sup>, Jun J. Liou<sup>a,b,c</sup>, Yuhuai Liu<sup>a,b,c,d</sup>\*

<sup>a</sup>Zhengzhou University, School of Electrical and Information Engineering, National Center for International Joint Research of Electronic Materials and Systems, International Joint-Laboratory of Electronic Materials and Systems of Henan Province, Zhengzhou, Henan 450001, P. R. China.

<sup>b</sup>Zhengzhou University, Institute of Intelligence Sensing, Zhengzhou, Henan 450001, P. R. China.

<sup>c</sup>Zhengzhou University, Research Institute of Industrial Technology Co. Ltd., Zhengzhou, Henan 450001, P. R. China.

<sup>d</sup>Zhengzhou Way Do Electronics Co. Ltd., Zhengzhou, Henan 450001, P. R. China.

Received: October 13, 2022; Revised: March 24, 2023; Accepted: April 13, 2023

Superhydrophobic surfaces of conventional Ti-6Al-4V (TC4) titanium alloys facilitate drag reduction and anti-wear. However, the economical fabrication of a wear-resistant superhydrophobic Ti-10V-2Fe-3Al (TB6) titanium alloy for application in modern aerospace equipment remains to be achieved. Here, an efficient wear-resistant superhydrophobic TB6 titanium alloy surface using commercially available materials and processing equipment was fabricated through nanosecond laser texturing and facile chemical modification. The wettability of textured surfaces, including line and grid patterns, ablated at different laser scanning intervals were investigated and analyzed in terms of surface morphology and chemical composition. Moreover, the mechanisms of coefficient of friction changes on different surfaces under dry and water sliding conditions were studied based on surface morphology and wettability. Under dry sliding and water lubrication conditions, the average coefficient of friction of the prepared superhydrophobic surface can be reduced by 29% and 74%, respectively, compared with that of the original hydrophilic surface.

**Keywords:** *Laser texturing, TB6 titanium alloy, surface morphology, superhydrophobic, tribological properties.*

### Introduction

Ti-6Al-4V (TC4) titanium alloys have high specific strength, optimal toughness, and corrosion resistance<sup>1-3</sup> and have been widely used for the manufacture of aircraft landing gear, engine compartment, tail wing, and main bearing rotating structural components of the helicopter rotor system<sup>4-6</sup>. A typical low-cost proximity  $\beta$ -titanium alloy (Ti-10V-2Fe-3Al or TB6) can reduce the mass of air vehicles by approximately 20%<sup>7-9</sup> compared to a TC4 titanium alloy in aeronautic manufacturing. However, aircrafts are often impacted by flying stones during takeoff and landing, and their structural components are highly susceptible to loss of efficacy due to friction and wear under the long-term accumulation effect<sup>10</sup>. Furthermore, in the joints of a helicopter rotor system under high-frequency alternating loads, the interaction between the central part of the main rotor hub and the surrounding lug connectors lead to severe fretting wear. This results in a significant reduction in fatigue strength and service life<sup>11</sup>. In addition, when an aerial vehicle is exposed to a highly humid environment, its surface is prone to water condensation, which cannot be timely removed from the surface of the air vehicle. Consequently, long-term water contact with various components of the air vehicle leads to corrosion<sup>12</sup>. Therefore, many surface techniques have been developed in recent years to prepare superhydrophobic wear-

resistant titanium alloy surfaces<sup>13-15</sup>. Ma et al.<sup>16</sup> prepared Cr coating with micro-nano porous structure on TC4 titanium alloy substrate using plasma reverse sputtering process, which significantly improved the surface wear resistance, hydrophobicity, and adhesion. Chen et al.<sup>17</sup> fabricated high roughness Al coating on TC4 titanium alloy surface via thermal spray technique. They obtained a surface with superhydrophobicity after polytetrafluoroethylene immersion and high temperature sintering, which remained hydrophobic with  $> 140^\circ$  water contact angle (WCA) after strong friction. Meng et al.<sup>18</sup> obtained low adhesion and superhydrophobicity on the surface of TC4 titanium alloy substrate using a method of TiO<sub>2</sub>/Ni composite electrodeposition combined with the self-assembly of a tridecafluorooctyltriethoxysilane molecular film. They achieved an average coefficient of friction (CoF) reduction of 25%. However, practical applications of wear-resistant titanium alloy surfaces are limited by production cost because their fabrication requires special equipment or metal-based materials other than the substrate materials as coating. Additionally, these studies are mostly based on TC4 titanium alloys, and relevant research on the TB6 Ti alloy is lacking. Thus, this study attempted to address this research gap by ablating periodic array morphology including line and grid patterns on the TB6 titanium alloy surface using a laser marking machine. Consequently, a superhydrophobic titanium alloy surface was obtained by immersion with

\*e-mail: [ieyhliu@zzu.edu.cn](mailto:ieyhliu@zzu.edu.cn)

octadecyltrichlorosilane (OTS) solution. The wettability and tribological properties of the samples were characterized using a video optical contact angle system and a universal mechanical tester. Surfaces with superhydrophobicity, with an average CoF reduction of 29% and 74% under dry friction and water lubrication conditions, respectively, were obtained compared to the original hydrophilic surface. The proposed method in this study offers the advantages of cost effectiveness, high efficiency, good reproducibility, and low cost. Moreover, it is expected to provide a theoretical basis for the large-scale production of superhydrophobic wear-resistant TB6 titanium alloy workpieces.

## 1. Experiment

Figure 1 shows the preparation method of the superhydrophobic TB6 titanium alloy surface. All materials and equipment used in the experiments were commercially obtained. The TB6 titanium sheet of size 30 mm × 30 mm × 3 mm was selected as the substrate material for the study samples and was mechanically polished until the surface roughness ( $S_a$ , arithmetic mean height) was less than 0.1  $\mu\text{m}$ . First, the samples were successively ultrasonically cleaned using petroleum ether, absolute ethanol of analytical-reagent grade, and deionized water prepared in the laboratory for 2 min. Second, a laser marking machine (KF-50L, Sundor, China), consisting of a nanosecond pulsed laser (P50QB, Raycus, China) with a central wavelength of 1064 nm and a pulse width of 130 ns, was used to ablate and pattern titanium alloy surfaces. The laser beam was concentrated via an F- $\theta$  lens with a focal length of 254 mm, and a spot diameter of approximately 100  $\mu\text{m}$  was projected on the sample. The laser process parameters, namely, power output, repetition rate, and scanning speed, were set to 45 W, 60 kHz, and 500 mm/s, respectively. To fabricate textured surfaces with different densities of line and grid patterns, the laser scanning intervals were selected as 100, 150, 200, 250, 300, 350, and 400  $\mu\text{m}$ . Third, the laser-treated titanium alloy samples were placed approximately 10 cm from a 250 W ultraviolet (UV) high-pressure mercury lamp with a center wavelength of 365 nm and continuously irradiated for 1 h for surface hydroxylation. Afterward, the samples were soaked in 3 wt.% OTS solution for 2 h for chemical surface

modification. Finally, the samples were ultrasonically cleaned using petroleum ether, anhydrous ethanol, and deionized water for 2 min. Thereafter, a hairdryer (FH6618, FLYCO, China) was used to fully blow dry the titanium alloy surface to complete the preparation of samples.

The surface morphologies of the samples were observed via scanning electron microscopy (SEM, Verios 5 UC, Thermo Fisher Scientific, USA). Confocal laser microscopy (LEXT OLS5100, Olympus, Japan) was used to survey and measure the surface contours and  $S_a$  of the samples. The chemical composition of the sample surface was analyzed using energy dispersive spectrometry (EDS, UltimMax100, Oxford Instruments, England). The contours of 3  $\mu\text{L}$  droplets of deionized water were automatically captured through optical contact angle measurements and contact analysis systems (OCA25, DataPhysics, Germany), and the Laplace-Young equation<sup>19</sup> was used to calculate the static WCA at the sample surface. Further, the WCA at five different locations on various surfaces was measured to evaluate the surface wettability. The instantaneous CoF on the sample surface was recorded in real time by performing a linear reciprocating friction test based on a ball-plate type universal tribometer (umt-5, Bruker, USA). To simulate the working environment of aerial vehicles and evaluate the possibility of using water as a lubricant, the test was performed under dry friction conditions and deionized water lubrication. A  $\text{Si}_3\text{N}_4$  ball with a diameter of 10 mm was selected as the friction pair. During the trial, titanium alloy samples were maintained stationary; the friction pairs were subjected to reciprocating sliding with a load of 1 N, and a single straight sliding pass of 6 mm and frequency of 1 Hz were applied for 600 s. Subsequently, the average CoF during sliding was calculated. Moreover, each surface was subjected to a set of trials under separate sliding conditions, and each set of trials was repeated three times to ensure effective statistical significance.

## 3. Results and Discussion

The surface of TB6 titanium alloy was ablated based on a groove structure by a continuously moving pulsed laser. As shown in Figure 2, for a single groove, the cross-section profile was U-shaped with depth and width of  $19.2 \pm 1.4$  and

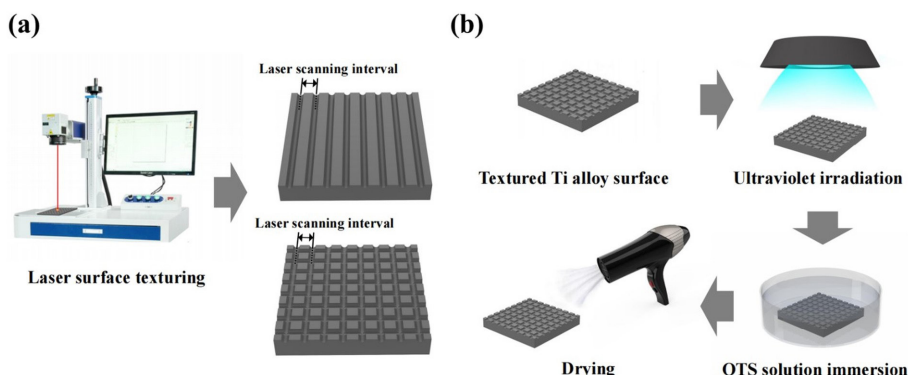


**Figure 1.** Schematic of the preparation process for superhydrophobic TB6 surfaces: (a) laser surface texturing, and (b) surface chemical treatment.

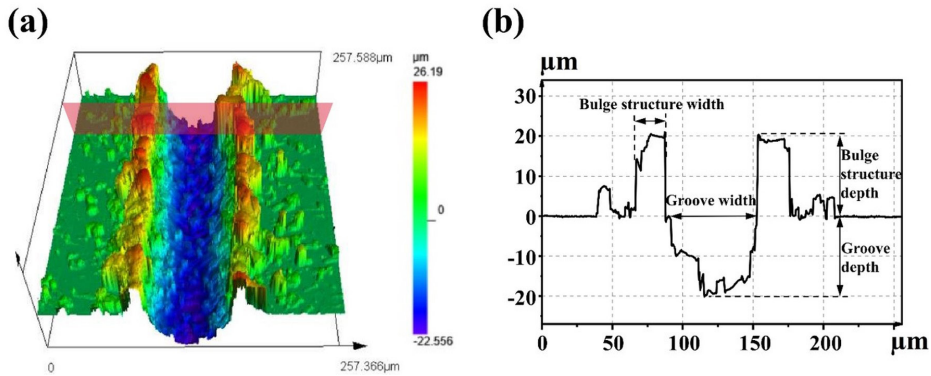


**Figure 2.** (a) Three-dimensional profile, and (b) profile line of a single groove ablated by a laser.

$66.1 \pm 3.9 \mu\text{m}$ , respectively. Further, the edges on both sides of the groove harbored micro bulge structures formed by self-deposition of the material melts with height and width of  $21.4 \pm 1.9$  and  $27.1 \pm 4.4 \mu\text{m}$ , respectively.

The morphologies of the titanium alloy surfaces after laser treatment with the same laser process parameters were controlled by the patterns composed of different arrangements of grooves. Figure 3 shows SEM images and profiles of textured surfaces with line and grid patterns at laser scanning intervals of 100, 250, and 400  $\mu\text{m}$ . When the laser scanning interval was 100  $\mu\text{m}$  (Figure 3a, 3d), the gap between grooves on the surface of line pattern texture was covered by mutually stacked bulge structures. The distance from the top of the bulge structure to the bottom of the groove reached  $50.5 \pm 1.7 \mu\text{m}$ , which was greater than  $40.3 \pm 1.7 \mu\text{m}$  in case of a single groove. Moreover, several nano-scale particle structures were distributed on the internal surface of the groove. During laser treatment, a considerable amount of heat generated by the laser was concentrated at a single point in a nanosecond transient pulse, and the titanium alloy surface was rapidly melted. Owing to the constant movement of the laser beam, the effect from the high spot size overlap enhanced the splash of the molten substance, thereby causing large particle and small debris spatters to fall back onto the surface and be re-solidified quickly. Consequently, they formed a micro-nano composite structure inside the groove<sup>20</sup>. For surfaces textured by grid patterns, rod-shaped bulge structures formed by strong material stacking effects were generated near the intersection of the laser processing pathways as the chains of bulge structures between the grooves were remelted again. With increase in the laser scanning interval (Figure 3b-3c, Figure 3d-3e), gradually sparse array structures composed of single grooves were observed on the surfaces of both the pattern textures, and spatters with gradually decreasing distribution density were distinguishable from untextured areas on the surface. However, for surfaces with grid pattern textures, dimples deeper than a single groove appeared at the intersection of laser processing paths, and the strong stacking effect of remelts near the intersection was weakened.

The variation in Sa of samples with laser scanning interval is shown in Figure 4. The Sa of the surfaces textured by both the line and grid patterns decreased approximately linearly and monotonously with increasing laser scanning interval.

At the same laser scanning interval, the Sa of the surface textured by the grid pattern was invariably larger than that of the surface textured by the line pattern. This can be attributed to the laser number of groove structures being laser ablated during the texturing process of preparing the grid pattern.

The surface chemical composition and WCA of the various samples are shown in Figure 5. After laser treatment and UV irradiation, the WCA on the surface of TB6 titanium alloy decreased from original hydrophilicity of  $82.2^\circ$  to superhydrophilicity of approximately  $0^\circ$ . Further, the O element content on the surface increased from 3.86 to 12.11 wt.%. In addition, strong oxidation reaction occurred during the process of laser ablation and a large amount of metal oxides were formed on the titanium alloy surface<sup>21</sup>. The oxygen holes on the metal surface are replaced by  $\text{H}_2\text{O}$  molecules in air to form hydroxyl groups. Moreover, under the UV catalysis, oxygen molecules in the atmospheric environment are decomposed into ozone molecules and oxygen atoms, wherein oxygen atoms combine with water molecules to form strongly oxidized hydroxyl groups on metal surfaces. These reactions result in significant increase of the free energy on the surface of titanium alloys<sup>22</sup>. The sample after laser treatment (grid patterned texture, 400  $\mu\text{m}$  laser scanning interval) was immersed in OTS solution, whose molecules underwent a dehydration condensation reaction with the hydroxyl groups on the surface of titanium alloy and successfully assembled itself onto the material surface. Subsequently, they endowed the sample surface with superhydrophobicity with a WCA of  $153^\circ$ . In addition, the detected emerging Si element of 0.8 wt.% for surface chemical composition verified that OTS molecules were successfully assembled. In comparison, the original surface showed hydrophobicity with a WCA of  $107.1^\circ$  after OTS treatment only, while only Si elements of 0.07 wt.% were observed, which indicated that the roughening of the surface contributed to the adhesion of more OTS molecules to the surface and thus to the formation of superhydrophobic surfaces.

The WCA of various chemically treated textured surfaces varied with the laser scanning interval, as shown in Figure 6. For the surface textured via the line pattern, the maximum WCA of  $154.1^\circ \pm 1.4^\circ$  was observed at laser scanning interval of 100  $\mu\text{m}$ . Similar to the change in Sa, the WCA decreased with increasing laser scanning interval;



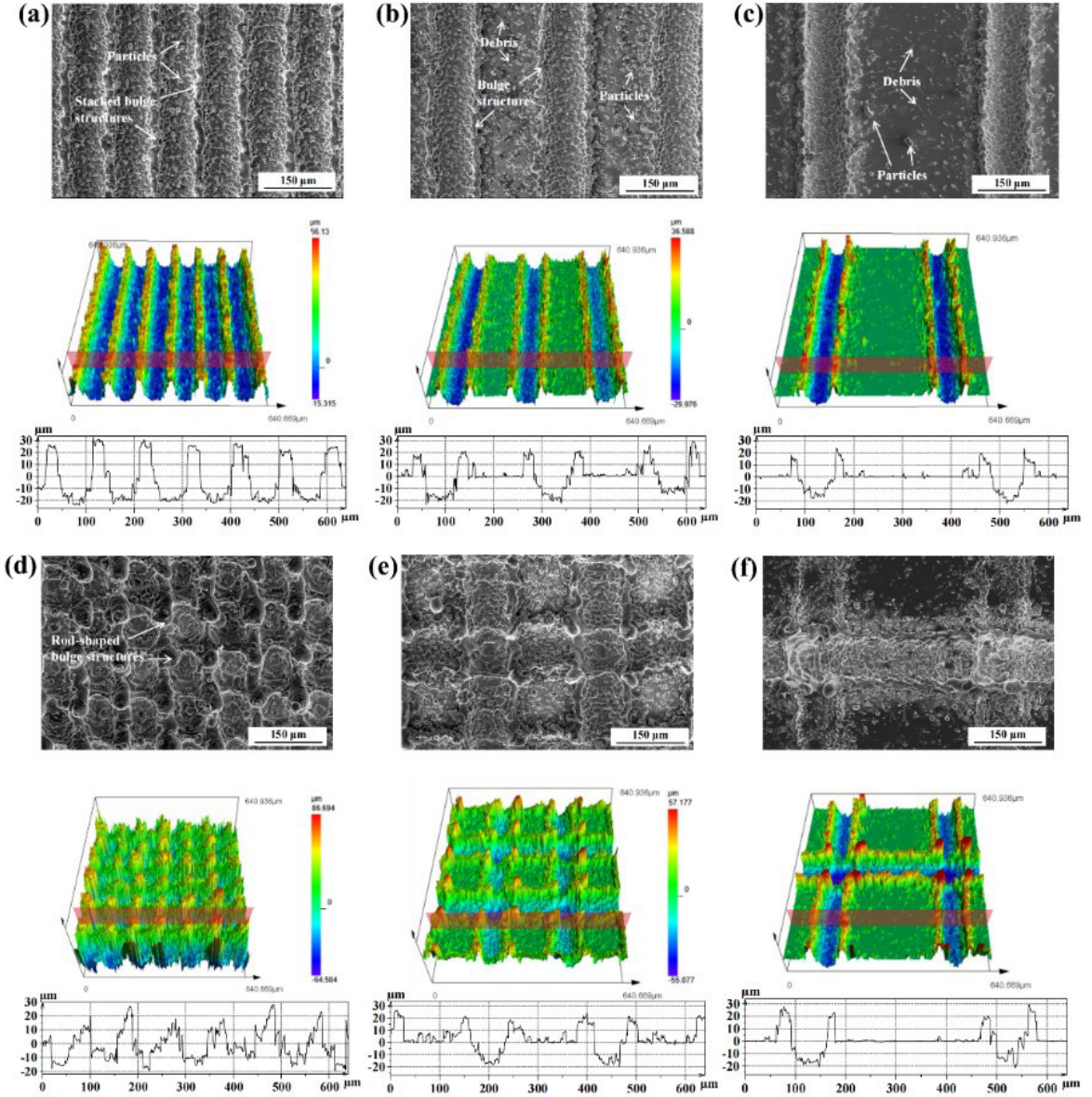


**Figure 3.** SEM image, three-dimensional profile, and profile lines of a line pattern textured surface with laser scanning intervals of (a) 100  $\mu\text{m}$ , (b) 250  $\mu\text{m}$ , and (c) 400  $\mu\text{m}$ , and a grid pattern textured surface with laser scanning intervals of (a) 100  $\mu\text{m}$ , (b) 250  $\mu\text{m}$ , and (c) 400  $\mu\text{m}$ ; the red-marked surface on the three-dimensional profiles indicates the measuring position of the profile lines.

however, the trend followed was different. In the range of laser scanning interval from 100 to 250  $\mu\text{m}$ , the sample surfaces maintained superhydrophobicity and the WCA decreased slowly. When the laser scanning interval reached 300  $\mu\text{m}$ , the superhydrophobicity of surface wettability was lost and transformed to hydrophobicity, and the WCA decreased sharply to  $140^\circ \pm 2^\circ$  of hydrophobicity. With the gradual increase in laser scanning interval, the WCA eventually decreased to  $122.5^\circ \pm 2.3^\circ$  at 400  $\mu\text{m}$  with a rapid change. According to the model proposed by Cassie and Baxter<sup>23</sup>, the droplet interacts with the surface micro-structure while in contact with the solid surface. The WCA satisfies the following equation

$$\cos\theta = f_1 \cos\theta_1 + f_2 \cos\theta_2 \quad (1)$$

where  $\theta$  is the WCA observed on the textured surface;  $\theta_1$  and  $\theta_2$  are the intrinsic WCAs of air and ideal smooth original solid surface, respectively, and  $f_1$  and  $f_2$  are the area proportional fractions of air-liquid and solid-liquid interfaces, respectively. As  $\theta_1 = 180^\circ$  and  $f_1 + f_2 = 1$ ,  $\theta$  decreases when  $f_2$  increases or  $f_1$  decreases. For a large laser scanning interval, the sparse grooves allow droplets extremely easy access to the inside of the grooves, resulting in a larger solid-liquid area percentage and thus a smaller WCA. For the surface textured by grid pattern, stable superhydrophobicity can

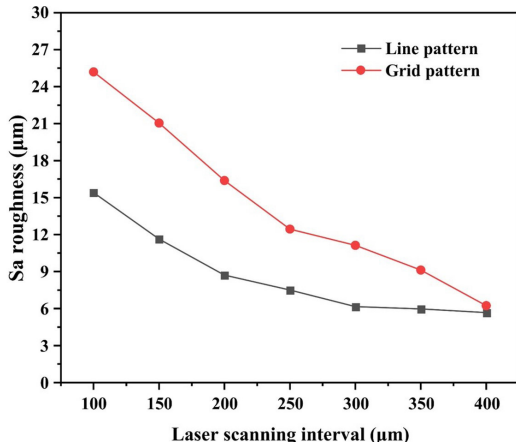


**Figure 4.** Variation in sample surface roughness with laser scanning intervals.

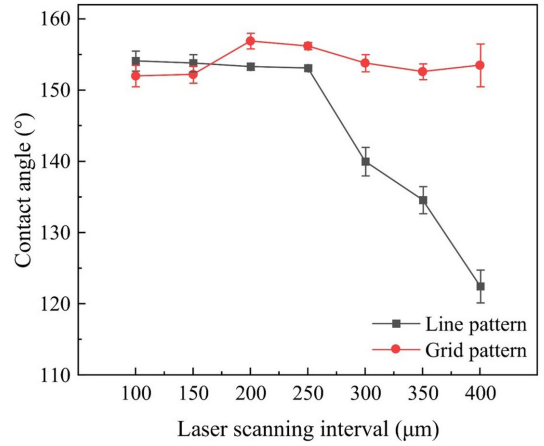


**Figure 6.** Variation in the water contact angle of the sample surface with laser scanning intervals.

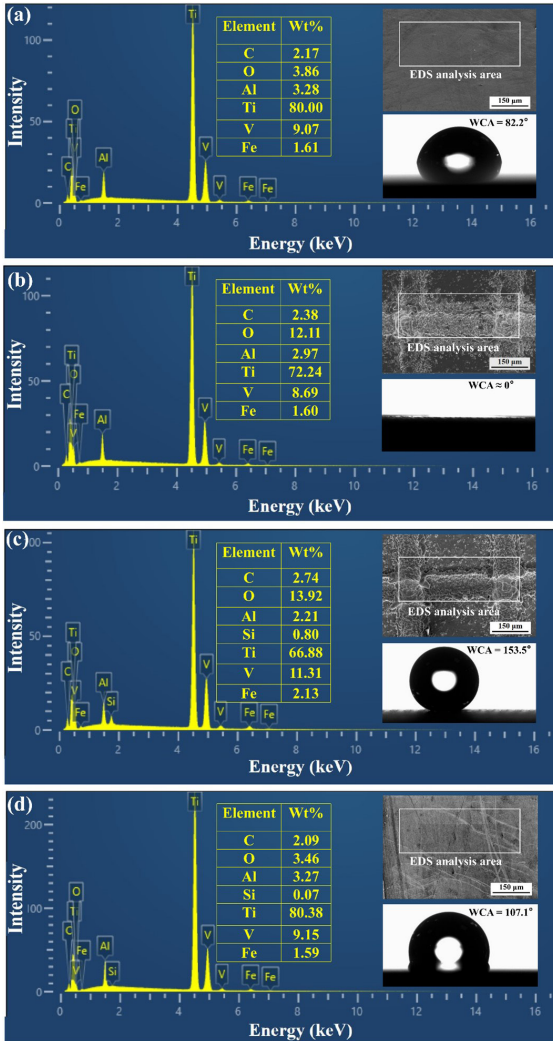


**Figure 5.** EDS spectra of TB6 titanium alloy: (a) original surface, (b) textured surface, (c) chemically treated textured surface, and (d) chemically treated original surface.

be sustained for laser scanning interval range of 100 to 400 µm, and a maximum of  $156.9^\circ \pm 1.1^\circ$  WCA was generated when the laser scanning interval was 200 µm. The compact laser scanning interval below 200 µm resulted in abrupt rod-shaped bulge structures and was immersed in contact with the droplet and thus limited the WCA. When the laser scanning interval ranged from 200 to 400 µm, WCA decreased with the increase in laser scanning interval. Previous studies have confirmed that WCA increases with the increase in Sa on the sample surface<sup>24</sup>. Therefore, the surface textured by the grid pattern under the same laser scanning features a larger WCA along with a larger Sa. However, although WCA exhibits a correlation with Sa, surfaces with larger Sa need not always result in larger WCA. Sa is only an indicator to evaluate the surface morphology, and WCA is regulated by the specific characteristics of the surface morphology.

Figure 7a shows the average CoF of the original and textured surfaces under dry friction conditions. The average CoF of the original surface against the  $\text{Si}_3\text{N}_4$  ball was 0.549. For laser scanning interval of 100 µm, the average CoF of the surface textured by the line and grid patterns were greater than that of the original surface, that is, 0.552 and 0.592, respectively. With increase in the laser scanning interval, the average CoF of the surface textured by both patterns first decreased and then increased. For the surfaces textured by line pattern, the average CoF of the surface was less than that of the original surface for laser scanning interval range of 150 to 400 µm, and the minimum average CoF of 0.39 was obtained at laser scanning interval of 200 µm. When the grid shape was a texture pattern, for surfaces with laser scanning intervals set to 150, 200, and 250 µm, the average CoF was smaller than that of the original surface, and the minimum average CoF of 0.484 was measured at a scanning interval of 250 µm. However, the average CoF of the textured surface was larger than that of the original surface in the range of laser scanning spacing from 300 to 400 µm. According to the equation presented by Suh and Sin<sup>25</sup>, CoF should be expressed as:  $\text{CoF} = \mu_1 + \mu_2 + \mu_3$ , where  $\mu_1$ ,  $\mu_2$ , and  $\mu_3$  are CoF caused by plowing, adhesion, and asperity contact, respectively.

$\mu_1$  and  $\mu_2$  are positively correlated with the actual contact area between the friction pair and the surface, whereas  $\mu_3$  is correlated with the surface roughness<sup>26</sup>. With increase in the laser scanning interval, the distribution density of the grooves decreased; the actual contact area between friction pair and surface increased, and plowing and adhesion became the dominant factors affecting CoF. Consequently, the average CoF increased. Moreover, benefiting from the capture effect of the grooves, dense grooves aid in accommodating more wear debris generated during sliding<sup>27</sup>. However, the densely arranged grooves cause excessive surface undulation, which implies larger Sa. The friction pair preferentially contacts and collides with the bulge structure on the surface when sliding, prompting the deformation mechanism of the material to transform from elastic to plastic, which leads to a significant increase in friction<sup>28</sup>. For the same laser scanning interval condition, when the surface textured by the grid pattern slid against the  $\text{Si}_3\text{N}_4$  ball, more bulge structures existing on the surface were touched by the  $\text{Si}_3\text{N}_4$  ball. Consequently, the average CoF exhibited a higher value than the line pattern textured surface.

Figure 7b shows the average CoF of the original and textured surfaces under water lubrication. As water also flushes the debris while reducing the shear strength between two sliding solid surfaces<sup>29</sup>, the average CoF of the original surface was measured as 0.493, which was less than the average CoF of the original surface under dry friction. Similar to the trend of the average CoF under dry friction condition, the surfaces textured by the line and grid patterns at 100  $\mu\text{m}$  laser scanning interval yielded average CoFs of 0.525 and 0.518, which were larger than in the original surface; the average CoF of the surface textured by the line and grid patterns first decreased and then increased with the increase in laser scanning interval. The smallest average CoFs of 0.129 and 0.252 were obtained at laser scanning intervals of 200 and 250  $\mu\text{m}$ , respectively. For the same surface, the average CoF under water lubricating condition was less than that under dry friction condition. The grooves on the textured surfaces contributed to hydrodynamic lubrication under water sliding conditions, which allowed the load-bearing capacity of the sample surface to be improved<sup>30</sup>. According

to the equation proposed by Jung and Bhushan<sup>31</sup>, the friction pair exerts a force

$$F = \pi R \gamma (\cos\theta_s + \cos\theta_f) \quad (2)$$

perpendicular to the downward direction of the contact surface on the sample surface when sliding back and forth, where  $\theta_s$  and  $\theta_f$  are the contact angles of lubricating medium for sample surface and friction pair surface, respectively,  $R$  is the diameter of the friction pair, and  $\gamma$  is the surface tension of the lubricating medium. When water (with a surface tension of approximately 72 mN/m at 25 °C) is used as the lubricant, the superhydrophobic surface causes weak or even side-effect  $F$  to be produced, which reduces the surface adhesion and friction. Thus, benefiting from the super hydrophobicity of the surface, when the laser scanning interval was within the range of 150 to 400  $\mu\text{m}$ , the surface textured by the grid pattern always maintained an average CoF of less than 0.4 under the condition of water lubrication. Further, when the laser scanning interval was set to 150 and 200  $\mu\text{m}$ , the average CoFs of 0.169 and 0.129 were obtained for the surface textured with line pattern, which were smaller than 0.378 and 0.262 for the surface textured with grid pattern, respectively. Thus, the CoF is the manifestation of multiple influencing factors working together while competing among themselves, with superhydrophobicity being the primary factor affecting CoF. Thus, under dry friction and water lubrication conditions, the average CoF on superhydrophobic textured surfaces decreased from 0.549 and 0.493 to 0.39 and 0.129, respectively, which corresponded to decrease of 29% and 74% compared to that of the original surface.

Figure 8a shows the instantaneous CoF changes of the original surface and the surface textured by the line pattern groove at 200  $\mu\text{m}$  interval at 600 s under dry friction and water lubrication conditions; the corresponding SEM images of wear track are also shown. To better observe the morphology of wear tracks, the samples were washed using ultrasonic wave for 2 min successively in the environment of absolute ethanol and ionized water before performing the SEM analysis. For the original surface, CoF under both sliding conditions increased above 0.5 at the beginning of

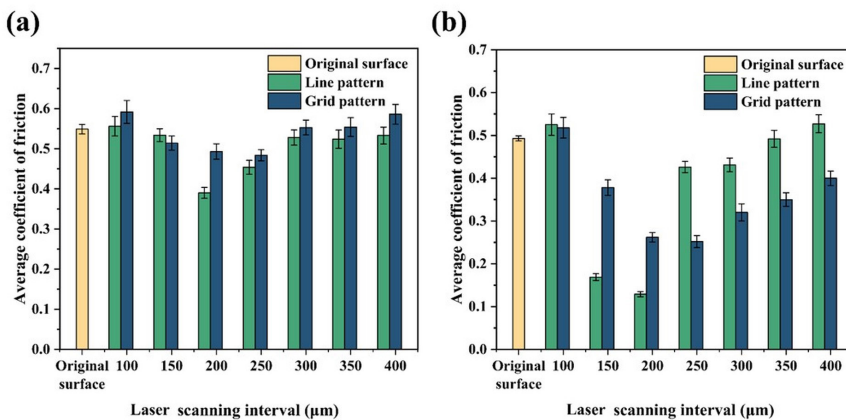
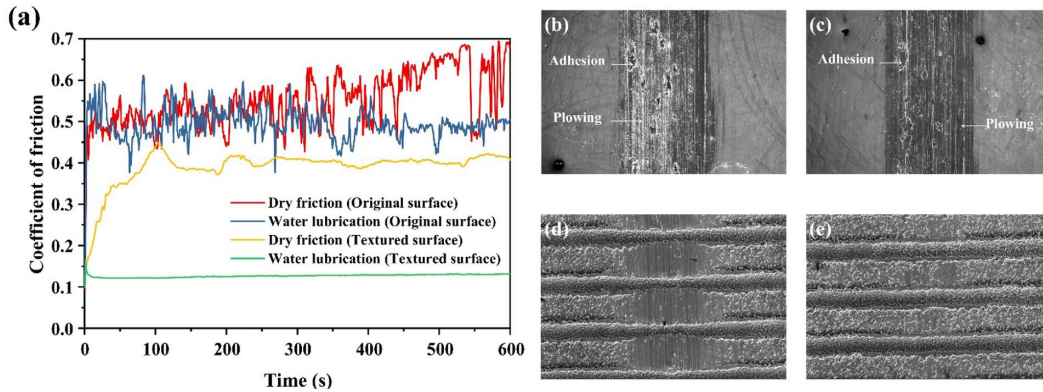


Figure 7. Average CoF of the original surface and textured surface under (a) dry friction and (b) water lubrication conditions.





**Figure 8.** (a) Variation in CoF with sliding time on the original surface and textured surface (line pattern, 200  $\mu\text{m}$  laser scanning interval) under dry friction and water lubrication conditions. Wear track on original surface under (b) dry friction, (c) water lubrication, and textured surface under (d) dry friction and (e) water lubrication.

the sliding process and showed a similar trend in the range of sliding time from 0 to 300 s, that is, random fluctuation in the range of 0.4 to 0.6. This indicated the poor wear resistance of the TB6 titanium alloy. When the sliding time was in the range of 300 to 600 s, the CoF under the dry friction condition showed a constant trend of increasing concussion until it approached 0.7. The wear track surface exhibits deep furrows and adhesive wear causes more debris to adhere to each other (Figure 8b), which can be primarily attributed to the following two aspects. First, the low plastic shear resistance of the titanium alloy surface<sup>32</sup> and the plowing action of hard  $\text{Si}_3\text{N}_4$  balls on the soft structure caused severe material loss and resulted in deep furrows on the surface. Second, abundant wear debris formed on the surface of titanium alloy was extruded from the friction contact surface, and certain debris were stuck and transferred to the surface of the friction pair, which were repeatedly rolled and deformed in the process of sliding and adhered to the surface of the wear debris<sup>33</sup>. The CoF of the original surface under the water lubrication condition was maintained at approximately 0.5, which benefited from the timely scouring of the debris by water. Although the friction mechanism of the surface at this time is mainly adhesive wear based on the wear tracks, the plowing and adhesion effects were reduced. For the surface textured by the line pattern with 200  $\mu\text{m}$  laser scanning interval, the friction pair first contacted the protrusive structure on the surface of the Ti Alloy during the sliding process under the dry friction condition. Further, its CoF increased from 0.1 to 0.45, exhibiting an approximately linear trend from 0 to 100 s. Subsequently, it benefited from the wear debris capture, adhesion, and plowing of the textures, and CoF decreased to approximately 0.4 for the range of 100 to 150 s and maintained a slight floating point at this value after 150 s, which continued until the end of the experiment. The wear track appears to be shallower, and a portion of the trench is worn; the worn form of the surface is dominated by abrasive wear (Figure 8c). Under water lubrication conditions, a continuous water film with superhydrophobicity was formed on the surface, and the CoF remained stable at approximately 0.13 for the entire test duration. Moreover, the wear track shows that only the

bulge structures and surface particles near the grooves on the surface are slightly worn (Figure 8d). The wear tracks from the SEM images were only visually evaluated for convenience. Recently, an analysis based on advanced microscopy with digital image processing has been used to evaluate the surface integrity<sup>34</sup>, which is encouraged in future studies for a more accurate qualitative measurement of surface topography and establish a correspondence between the surface morphology of the textured TB6 surface and the CoF changes under different conditions.

## 4. Conclusion

A wear-resistant superhydrophobic surface of the TB6 titanium alloy was fabricated via laser-texturing technology and a simple chemical modification method based on all-commercial processing equipment and materials. This study explored laser texturing on TB6 titanium alloys and was not limited to only commonly examined TC4 titanium alloys. The surface texture patterns included line and grid patterns. WCA and CoF were used to evaluate the wettability and tribological properties of the sample surfaces. The surface morphology and chemical composition of the samples were analyzed and were used to explain the changes in surface wettability and tribological properties. Further, the morphology of the wear track surface was used to verify the wear mechanism. The main conclusions of this study are as follows:

- (1) The micro-groove with bulge structures at the edges, which were ablated to fabricate different textured surfaces, were attributed to the laser heat effect. The splashes of particle structure and debris were randomly dispersed at the bottom of the micro-groove structure and on the untextured surface, forming a micro-nano composite structure with the micro-groove. The surface roughness increased with the decrease in laser scanning interval for surfaces textured by line and grid patterns.
- (2) During laser texturing, the hydrophilic TB6 titanium alloy surface underwent strong oxidation reactions, and the surface exhibited superhydrophilicity. After the OTS solution immersion, the textured

surface showed strong hydrophobicity and even superhydrophobicity, compared with the untextured surface which exhibited a weaker hydrophobicity. This indicated that a rough surface was conducive to the self-assembly of an OTS molecular film.

- (3) The textured surfaces with higher Sa exhibited higher WCA after chemical treatment, and the maximum WCA with superhydrophobicity of  $156.9^\circ \pm 1.1^\circ$  was readily obtained when the surface was textured by a grid pattern at a laser scanning interval of 200  $\mu\text{m}$ . However, the surface textured by grid patterns under lower scanning intervals of 100  $\mu\text{m}$  and 150  $\mu\text{m}$  limited further increases in WCA owing to the strong bulge structure of the surface.
- (4) The tribological properties of the titanium alloy surface were influenced by factors such as surface topography, surface Sa, and actual contact area between surface and friction pair during dry friction, and the surface wettability additionally affected the tribological properties under water lubrication conditions. As the laser scanning interval increased, the average CoF of the surface textured by the line and grid patterns first decreased and then increased under both sliding conditions. Benefited from surface roughness and hydrophobicity, the surface with appropriate texture could obtain wear resistance. Among them, the surface textured by line patterns at a laser scanning interval of 200  $\mu\text{m}$  showed the best wear resistance, with the average CoF of 0.39 and 0.123 under dry friction and water sliding conditions, respectively, which were 29% and 74% lower than that of the original surface.

The proposed fabrication method for wear-resistant superhydrophobic titanium alloy has low cost, is highly efficient, is highly repeatable, and does not require metal-based materials other than the substrate materials as coating, which extends the potential application in the TB6 titanium alloy workpieces. However, the findings and conclusions of this study are based on experimental phenomena. Therefore, theoretical calculation and numerical simulation of the wear reduction mechanism of hydrophobic textured surfaces need further study.

## 5. Acknowledgements

This work was supported by the National Nature Science Foundation of China (no. 62174148), National Key Research and Development Program (no. 2022YFE0112000; no. 2016YFE0118400), Zhengzhou 1125 Innovation Project (no. ZZ2018-45), and Ningbo 2025 Key Innovation Project (no. 2019B10129).

## 6. References

1. Cui C, Hu BM, Zhao L, Liu S. Titanium alloy production technology, market prospects and industry development. *Mater Des.* 2011;32(3):1684-91.
2. Sharma D, Mohanty S, Das AK. Surface modification of titanium alloy using hBN powder mixed dielectric through micro-electric discharge machining. *Surf Coat Tech.* 2020;381:125157.
3. Ji R, Wang H, Wang B, Jin H, Liu Y, Cheng W et al. Removing loose oxide layer and producing dense  $\alpha$ -phase layer simultaneously to improve corrosion resistance of Ti-6Al-4V titanium alloy by coupling electrical pulse and ultrasonic treatment. *Surf Coat Tech.* 2020;384:125329.
4. Williams JC, Boyer RR. Opportunities and issues in the application of titanium alloys for aerospace components. *Metals.* 2020;10(6):705.
5. Kolli RP, Devaraj A. A review of metastable beta titanium alloys. *Metals.* 2018;8(7):506.
6. Özen İ, Gedikli H. Solid particle erosion on shield surface of a helicopter rotor blade using computational fluid dynamics. *J Aerosp Eng.* 2019;32(1):04018131.
7. Ma X, Chen Z, Xiao L, Luo S, Lu W. Stress-induced martensitic transformation in a  $\beta$ -solution treated Ti-10V-2Fe-3Al alloy during compressive deformation. *Mater Sci Eng A.* 2021;801:140404.
8. Li ZY, Liu XL, Wu GQ, Huang Z. Fretting fatigue behavior of Ti-6Al-4V and Ti-10V-2Fe-3Al alloys. *Met Mater Int.* 2019;25(1):64-70.
9. Boyer R, Briggs R. The use of  $\beta$  titanium alloys in the aerospace industry. *J Mater Eng Perform.* 2005;14(6):681-5.
10. Sastry YS, Kiros B, Hailu F, Budarapu P. Impact analysis of compressor rotor blades of an aircraft engine. *Front Struct Civ Eng.* 2019;13(3):505-14.
11. Davies D, Jenkins S, Belben F. Survey of fatigue failures in helicopter components and some lessons learnt. *Eng Fail Anal.* 2013;32:134-51.
12. Zolkin A, Galanskiy S, Kuzmin A. Perspectives for use of composite and polymer materials in aircraft construction. In: III International Conference on Advanced Technologies in Aerospace, Mechanical and Automation Engineering – MIST: Aerospace-III-2020; 2020 Nov 20-21; Krasnoyarsk, Russia. Proceedings. Bristol: IOP Publishing. p. 012023.
13. Li Q, Tang F, Wang C, Wang X. Facile fabrication of wear-resistant multifunctional surfaces on titanium alloy substrate by one-step anodization and modification with silicon dioxide nanoparticles. *J Sol-Gel Sci Technol.* 2016;80(2):318-25.
14. Zhao Y, Xu T, Hu J-M. A robust, room-temperature curable and molecular-level superhydrophobic coating with excellent antibacterial and antifouling properties. *Chem Eng J.* 2022;450(2):136557.
15. Xin G, Wu C, Cao H, Liu W, Li B, Huang Y et al. Superhydrophobic TC4 alloy surface fabricated by laser micro-scanning to reduce adhesion and drag resistance. *Surf Coat Tech.* 2020;391:125707.
16. Ma D, Lin H, Hei H, Ma Y, Gao J, Zhang M et al. Fabrication of porous micro/nano structured Cr coating with superhydrophobic and ultrahigh adhesion properties by plasma reverse sputtering process. *Vacuum.* 2022;201:111049.
17. Chen X, Gong Y, Suo X, Huang J, Liu Y, Li H. Construction of mechanically durable superhydrophobic surfaces by thermal spray deposition and further surface modification. *Appl Surf Sci.* 2015;356:639-44.
18. Meng J, Dong X, Zhao Y, Xu R, Bai X, Zhou H. Fabrication of a low adhesive superhydrophobic surface on Ti6Al4V alloys using  $\text{TiO}_2/\text{Ni}$  composite electrodeposition. *Micromachines.* 2019;10(2):121.
19. Zhang X, Shi F, Niu J, Jiang Y, Wang Z. Superhydrophobic surfaces: from structural control to functional application. *J Mater Chem.* 2008;18(6):621-33.
20. Li Z, Xue G, Wu Y, Wang X, Pan H. Preparation of superhydrophobic surfaces based on rod-shaped micro-structure induced by nanosecond laser. *Crystals.* 2021;11(11):1274.
21. Chang Y-Y, Zhang J-H, Huang H-L. Effects of laser texture oxidation and high-temperature annealing of TiV alloy thin films on mechanical and antibacterial properties and cytotoxicity. *Materials.* 2018;11(12):2495.
22. Bjelobrk N, Girard H-L, Subramanyam SB, Kwon H-M, Quéré D, Varanasi KK. Thermocapillary motion on lubricant-impregnated surfaces. *Phys Rev Fluids.* 2016;1(6):063902.



23. Cassie ABD, Baxter S. Wettability of porous surfaces. *Trans Faraday Soc.* 1944;40:546-51.
24. Wang J, Wu Y, Cao Y, Li G, Liao Y. Influence of surface roughness on contact angle hysteresis and spreading work. *Colloid Polym Sci.* 2020;298(8):1107-12.
25. Suh NP, Sin H-C. The genesis of friction. *Wear.* 1981;69(1):91-114.
26. Ding Q, Wang L, Hu L, Hu T, Wang Y. The pairing-dependent effects of laser surface texturing on micro tribological behavior of amorphous carbon film. *Wear.* 2012;274:43-9.
27. Ding X, Chen D, Zhang W, Yu S. Experiment of frictional vibration performance of the micro-texture of DLC thin film with dry gas seal rings. *Tribol Int.* 2020;147:106267.
28. Wang Z, Zhao Q, Wang C, Zhang Y. Modulation of dry tribological property of stainless steel by femtosecond laser surface texturing. *Appl Phys, A Mater Sci Process.* 2015;119(3):1155-63.
29. Mi X, Cai Z, Xiong X, Qian H, Tang L, Xie Y et al. Investigation on fretting wear behavior of 690 alloy in water under various temperatures. *Tribol Int.* 2016;100:400-9.
30. Costa H, Hutchings I. Hydrodynamic lubrication of textured steel surfaces under reciprocating sliding conditions. *Tribol Int.* 2007;40(8):1227-38.
31. Jung YC, Bhushan B. Contact angle, adhesion and friction properties of micro-and nanopatterned polymers for superhydrophobicity. *Nanotechnology.* 2006;17(19):4970.
32. Pan X, He W, Huang X, Wang X, Shi X, Jia W et al. Plastic deformation behavior of titanium alloy by warm laser shock peening: microstructure evolution and mechanical properties. *Surf Coat Tech.* 2021;405:126670.
33. Niu Y, Pang X, Yue S, Wang S, Song C, Shangguan B et al. Improving tribological properties of Ti–Zr alloys under starved lubrication by combining thermal oxidation and laser surface texturing. *Wear.* 2022;496:204279.
34. Carvalho S, Horovistiz A, Davim JP. Surface topography in machining Ti alloys for biomedical applications: correlative microscopy approach for qualitative and quantitative analysis. *Int J Adv Manuf Technol.* 2021;114:683-94.